Compactness of the ^{48}Ca induced hot fusion reactions and the magnitudes of quadrupole and hexadecapole deformations

Raj K. Gupta,[1,2] Monika Manhas,[1,2] and Walter Greiner[2]
[1]*Department of Physics, Panjab University, Chandigarh 160014, India*
[2]*Frankfurt Institute for Advanced Studies (FIAS), Johann Wolfgang Goethe Universität, Max-von-Laue-Str. 1, D-60438 Frankfurt am Main, Germany*
(Received 28 November 2005; published 15 May 2006)

Based on fragmentation theory extended to include the orientation degrees of freedom and higher multipole deformations up to hexadecapole deformations, the compactness of ^{48}Ca induced reactions on various actinides is studied for Ds ($Z = 110$) to 118 nuclei. It is shown that the reactions leading to $Z \geqslant 114$ nuclei are "compact" hot fusion reactions at $\theta = 90^\circ$ orientation angles (equatorial compact or ec; collisions that are in the direction of the minor axis of the deformed reaction partner), but the ones for $Z < 114$ nuclei are compact at $\theta < 90^\circ$ (not-equatorial compact or nec). The phenomenon of "barrier distribution in orientation degrees of freedom" is observed for the first time to be related to the magnitudes of both the quadrupole and hexadecapole deformations of the deformed reaction partner. The ec configurations are obtained for the cases of quadrupole deformation alone and with small (including negative values) hexadecapole deformations. The presence of large (positive) hexadecapole deformations result in the nec configurations. These results are found to be quite general, applicable also to other lighter targets such as W and Ra with the ^{48}Ca beam and to Pb based reactions. Furthermore, for compact hot fusion reactions, in addition to the ^{48}Ca reaction valley, a number of other new reaction valleys (target-projectile combinations) are obtained, the most important one (next to ^{48}Ca) being the ^{54}Ti nucleus used previously in Pb based cold fusion reaction studies but now proposed with deformed actinide nuclei such as ^{226}Ra, ^{232}Th, ^{238}U, and ^{242}Pu.

DOI: 10.1103/PhysRevC.73.054307 PACS number(s): 25.60.Pj, 25.70.Gh, 27.90.+b

I. INTRODUCTION

Using the fragmentation theory [1], extended to include the orientation degrees of freedom and higher multipole deformations within the generalized nuclear proximity potential [2,3], in a recent paper [4], we showed that $^{48}\text{Ca} + {}^{244}\text{Pu} \rightarrow {}^{292}114^*$ is a compact hot fusion reaction. For a hot fusion reaction, the barrier is highest and interaction radius smallest, which for the "compact" case occurs for collisions in the direction of the minor axis of the deformed reaction partner, i.e., for its 90° orientation (the "equatorial" configuration). We refer to such spherical+deformed configurations as the "equatorial compact" (ec) configurations. The basis for this result is the idea of "optimum orientations," which for coplanar nuclei are shown to be fixed by the signs of their quadrupole deformations alone, not affected by the signs of their hexadecapole deformations [1]. However, the magnitudes of both the quadrupole and higher-multipole deformations should also be important in the choice of different target-projectile combinations forming the (optimally oriented) compact hot compound system. This aspect of the problem has not been investigated much and is analyzed in this paper, taking the higher multipole deformations up to hexadecapole deformations. We have applied our considerations to ^{48}Ca induced hot fusion reactions, which resulted in successful synthesizing of the superheavy nuclei with Ds ($Z = 110$) to 118 (see, e.g., Refs. [5,6] and earlier references therein). We find that for $Z \geqslant 114$ nuclei, the reactions are compact at orientation angles $\theta = 90^\circ$, the above-noted ec configurations, whereas the same for $Z < 114$ nuclei occurs at $\theta < 90^\circ$, referred to simply as the "not-equatorial compact" (nec) configurations, to distinguish them from the ec configurations. The difference between the ec and nec configurations is found to be significantly large (~20°). Interestingly, the above results are found applicable to hot fusion reactions of even the unexplored region of $Z < 110$ nuclei, i.e., nuclei below Ds, using the ^{48}Ca or even Pb beam. The ec configurations for hot fusion (for $Z \geqslant 114$) refer to target nuclei having quadrupole deformations alone or with *small* hexadecapole deformations (including negative hexadecapole deformations). The larger positive hexadecapole deformation (for $Z < 114$), irrespective of the magnitude of quadrupole deformation, leads to $\theta < 90^\circ$, the nec configuration. Thus, in this paper, we have shown that for normal deformed nuclei, an explicit role is played by the magnitude of the hexadecapole deformation in hot fusion reactions. The octupole deformation is, in general, zero; but its contribution, whereever available, is also added in our final calculations of the fragmentation potentials for the choice of optimum compact target-projectile combinations for the hot fusion reactions.

Experimentally, the compactness in hot fusion reactions was observed by Oganessian *et al*. via the measured excitation functions, first in the $4n$ channel of the $^{48}\text{Ca} + {}^{244}\text{Pu} \rightarrow {}^{292}114^*$ reaction [5], and more recently in the $3n$ and $4n$ channels, respectively, of $^{48}\text{Ca} + {}^{238}\text{U} \rightarrow {}^{286}112^*$ and $^{48}\text{Ca} + {}^{242}\text{Pu} \rightarrow {}^{290}114^*$ reactions [6]. They noticed that compared to the well-studied ^{206,208}Pb based cold fusion reactions with excitation energy $E^* \sim 10$–20 MeV, the peaks of the excitation functions in these reactions are broader as well as shifted to higher excitation energies of $E^* \sim 35$–41 MeV, which could not be due to the dynamic limitations of fusion since the reaction partners involved in these reactions are rather

asymmetric. However, this effect could be associated with the static deformation of the target nucleus [6] and could arise if the collisions correspond to more compact configurations of the type of equator-cross [here "equatorial" (e), as one of the nucleus is spherical] since the barriers are higher by about 20 MeV, compared to the "elongated" pole-to-pole ("polar" for deformed+spherical cases) collisions. A higher barrier would mean an increased fusion threshold or increased number of emitted neutrons.

Theoretically, compact equator-cross or equatorial configurations have recently been envisaged by many authors [3,7–11]. Also, the role of hexadecapole deformation has been studied, mainly for its sign (positive or negative) and for the cold fusion reactions only [1,12,13]. For an equator-cross compact touching configuration of two well-deformed nuclei, some authors [9] suggest the use of nuclei with large negative hexadecapole deformations, whereas another [10] favors using the same with large positive values. The same situation has been presented in the calculations for the equatorial, spherical-plus-deformed combinations [12,13]. On the other hand, Manhas and Gupta [3] showed that the two equator-cross configurations, respectively, with positive or negative hexadecapole deformation, refer to cold or hot fusion reactions. For coplanar collisions (which also include the equatorial ones), however, Gupta *et al.* [1] found that the optimum orientations for both the cold and hot fusion processes are independent of the signs (+/−) of hexadecapole deformations and are decided by the sign (+, −, or zero) of quadrupole deformations alone. For the ^{48}Ca induced reactions, in a barrier distribution calculation, Misicu and Greiner [7] have shown that the inclusion of hexadecapole deformation enhances the probability of encountering a barrier at the equatorial configuration, compared to other orientations including the polar one. However, no study points out clearly the role of the magnitudes of either the quadrupole or the higher-multipole deformations for compact hot fusion reactions. We show in this paper for the first time that for deformed nuclei, negative hexadecapole deformation simply means a further reduction in the magnitude of small positive hexadecapole deformation below zero, and that it is the hexadecapole (β_4) deformation that plays the important role for a reaction to be an ec or nec hot fusion reaction. In other words, taking into account the magnitude of β_4, the cases of the equatorial compact and not-equatorial compact are separated out for the first time here, and the target-projectile (t-p) combinations (the "cold reaction valleys") for the hot fusion reactions are now identified on the basis of the (optimally oriented) compact (ec or nec) configurations.

The paper is organized as follows. The fragmentation theory recently extended to deformed and oriented nuclei is very briefly described in Sec. II. The results of our calculations for all the experimentally observed, ^{48}Ca based hot fusion reactions are presented in Sec. III. Also, applications of our method to hot fusion reactions in the domain of cold fusion reactions (Ca + Ra and Fe, Ge + Pb) and to lighter compound systems (e.g., W + Ca) are made in this section. Finally, a summary and discussion of our results is given in Sec. IV. We consider here only the case of nuclei lying in the same plane (coplanar nuclei; azimuthal angle $\phi = 0^\circ$).

II. THE EXTENDED FRAGMENTATION THEORY FOR DEFORMED AND ORIENTED NUCLEI

The extended fragmentation theory [1,4] writes the fragmentation potential in terms of the coordinates of mass and charge asymmetries $\eta = (A_1 - A_2)/(A_1 + A_2)$ and $\eta_Z = (Z_1 - Z_2)/(Z_1 + Z_2)$, the relative separation $\vec{R}$, the deformations $\beta_{\lambda i}$, $\lambda = 2$, 3, and 4, the quadrupole, octupole, and hexadecapole deformations of two nuclei ($i = 1$, 2), the two orientation angles θ_i, and the azimuthal angle ϕ between the principal planes of two nuclei as

$$V(\eta, \eta_Z, R) = -\sum_{i=1}^{2} B_i(A_i, Z_i, \beta_{\lambda i}) + V_C(R, Z_i, \beta_{\lambda i}, \theta_i, \phi) + V_P(R, A_i, \beta_{\lambda i}, \theta_i, \phi). \quad (1)$$

For coplanar nuclei, $\phi = 0^\circ$, and for spherical-plus-deformed nuclear collisions, only one orientation angle θ is enough, referring to the rotationally symmetric deformed nucleus.

In Eq. (1), B_i are the binding energies, taken from the calculations of Möller *et al.* [14] for $Z \geqslant 8$ (except otherwise stated) and from experimental data [15] for $Z < 8$. The Coulomb V_C and nuclear proximity V_P potentials for the $\phi = 0^\circ$ case are

$$V_C = \frac{Z_1 Z_2 e^2}{R} + 3Z_1 Z_2 e^2 \sum_{\lambda, i=1,2} \frac{1}{2\lambda+1} \frac{R_i^\lambda(\alpha_i)}{R^{\lambda+1}} Y_\lambda^{(0)}(\theta_i) \times \left[\beta_{\lambda i} + \frac{4}{7}\beta_{\lambda i}^2 Y_\lambda^{(0)}(\theta_i)\right], \quad (2)$$

and

$$V_P = 4\pi \bar{R} \gamma b \Phi(s_0), \quad (3)$$

where for the axially symmetric shapes,

$$R_i(\alpha_i) = R_{0i}\left[1 + \sum_\lambda \beta_{\lambda i} Y_\lambda^{(0)}(\alpha_i)\right], \quad (4)$$

with $R_{0i} = 1.28A_i^{1/3} - 0.76 + 0.8A_i^{-1/3}$, the specific surface energy constant $\gamma = 0.9517[1 - 1.7826\{(N-Z)/A\}^2]$ (in MeV fm^{-2}), the nuclear surface thickness $b = 0.99$ fm, and the universal function $\Phi(s_0)$, which depends only on the minimum separation distance s_0, is

$$\Phi(s_0) = \begin{cases} -\frac{1}{2}(s_0 - 2.54)^2 - 0.0852(s_0 - 2.54)^3, \\ -3.437 \exp\left(-\frac{s_0}{0.75}\right), \end{cases} \quad (5)$$

respectively, for $s_0 \leqslant 1.2511$ and $\geqslant 1.2511$. The minimized separation distance s_0 (in α_i), in units of b, for coplanar nuclei is defined [2] as (see Fig. 1)

$$s_0 = R - X_1 - X_2 = R - R_1(\alpha_1)\cos(\theta_1 - \alpha_1) - R_2(\alpha_2)\cos(180 + \theta_2 - \alpha_2), \quad (6)$$

with the minimization conditions

$$\tan(\theta_1 - \alpha_1) = -\frac{R_1'(\alpha_1)}{R_1(\alpha_1)}, \qquad \tan(180 + \theta_2 - \alpha_2) = -\frac{R_2'(\alpha_2)}{R_2(\alpha_2)}. \quad (7)$$

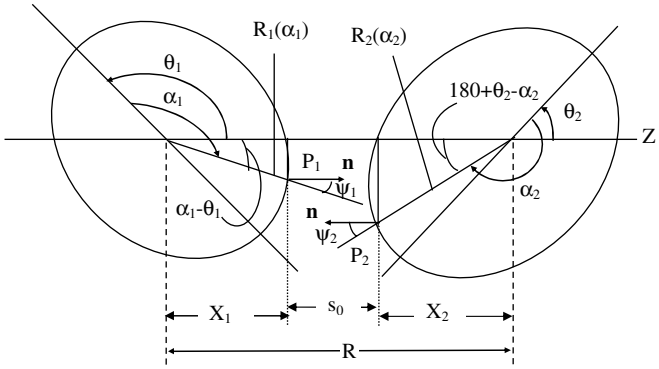

FIG. 1. Schematic configuration of any two axially symmetric deformed, oriented nuclei, lying in the same plane ($\phi = 0^\circ$).

Here, $R_i'(\alpha_i)$ are the first-order derivatives of $R_i(\alpha_i)$ with respect to α_i. The mean curvature radius $\bar{R}$, characterizing s_0, i.e., the points of closest approach for nuclei lying in the same plane ($\phi = 0^\circ$), is

$$\frac{1}{\bar{R}^2} = \frac{1}{R_{11}R_{12}} + \frac{1}{R_{21}R_{22}} + \frac{1}{R_{11}R_{22}} + \frac{1}{R_{21}R_{12}}, \qquad (8)$$

with R_{i1} and R_{i2} as the principal radii of curvatures at the two points of closest approach of nuclei (P_1 and P_2 in Fig. 1). For explicit expressions of R_{i1} and R_{i2} and other details, we refer the reader to [2].

We use the same formalism as above for noncoplanar nuclei ($\phi \neq 0^\circ$), but replace for the out-of-plane nucleus ($i = 1$ or 2) the corresponding radius parameter $R_i(\alpha_i)$ with its projected radius parameter $R_i^P(\alpha_i)$ in both the Coulomb and proximity potentials. For the proximity potential, it enters via the definitions of both the mean curvature radius $\bar{R}$ and the shortest distance s_0 [3]. The $R_i^P(\alpha_i)$ is determined by defining, for the out-of-plane nucleus, two principal planes $X'Z'$ and $Y'Z'$, respectively, with radius parameters $R_i(\alpha_i)$ and $R_j(\delta_j)$, such that their projections into the plane XZ of the other nucleus are (see Fig. 1 in Ref. [3])

$$R_i^P(\alpha_i) = R_i(\alpha_i)\cos\phi \qquad i = 1 \text{ or } 2, \qquad (9)$$

and

$$R_j^P(\delta_j) = R_j(\delta_j)\cos(\phi - \delta_j) \qquad j = i = 1 \text{ or } 2 \qquad (10)$$

Then, maximizing $R_j(\delta_j)$ in angle δ_j, we get

$$\begin{aligned} R_i^P(\alpha_i) &= R_i^P(\alpha_i = 0^\circ) + R_i^P(\alpha_i \neq 0^\circ) \\ &= R_j^P\left(\delta_j^{\max}\right) + R_i(\alpha_i \neq 0^\circ)\cos\phi, \end{aligned} \qquad (11)$$

with $\delta_j^{\max}$ given by the condition (for fixed ϕ),

$$\tan(\phi - \delta_j) = -\frac{R_j'(\delta_j)}{R_j(\delta_j)}. \qquad (12)$$

Thus, ϕ dependence of the projected radius vector $R_i^P(\alpha_i)$ is also contained in maximized $R_j^P(\delta_j^{\max})$. For further details, see Ref. [3]. Then, for nuclear proximity potential, denoting by V_P^{12} the potential for nucleus 1 to be out of plane and by V_P^{21} for nucleus 2 to be out of plane, the effective nuclear proximity potential, in view of the so-called kinematics independence of the reactions, is taken as

$$V_P = \tfrac{1}{2}\left[V_P^{12} + V_P^{21}\right]. \qquad (13)$$

Apparently, for the coplanar and identical (both nuclei the same) noncoplanar nuclei, $V_P^{12} = V_P^{21}$.

Finally, for fixed orientations, the charges Z_i in Eq. (1) are fixed by minimizing the potential in the η_Z coordinate, which fixes the deformations $\beta_{\lambda i}$ also. Then, Eq. (1) gives the fragmentation potential $V(\eta)$ for fixed R and, for its normalization to the binding energies, the scattering potential $V(R)$ for fixed η.

In fragmentation theory [16–21], the compound system is considered to be formed for *all* those t-p combinations that lie at the *minima* of $V(\eta)$ of a given compound nucleus, calculated for all possible t-p combinations. This information on potential energy minima (called, *cold reaction valleys*) is further optimized [22] by the requirements of the smallest interaction barrier, largest interaction radius, and nonnecked (no saddle) nuclear shapes. The orientations θ_i are also fixed for the optimum conditions of both the barrier heights and positions, which manifest themselves in the form of the following two criteria [1]: (i) the interaction radius is smallest, but the barrier is highest, which means a (most) compact hot nuclear shape, called the compact hot fusion configuration, and (ii) the barrier is lowest, but the interaction radius is largest, which means an elongated (noncompact) cold nuclear shape, called the elongated cold fusion configuration. Interestingly, in this paper we further find that for each t-p combination (studied here for spherical + deformed nuclei), the degree of compactness and/or elongation (referring to optimum orientation angles) depends on the magnitudes of hexadecapole deformations, its negative sign acting simply as weak (positive) magnitude below zero value. For reaction partners having quadrupole deformations alone, and with smaller hexadecapole deformations, the criteria for compactness and/or elongation are found to remain fixed, i.e., the optimum orientation angles are fixed, as in Table I of Ref. [1], and are not influenced by the (+/−) signs of their hexadecapole deformations. On the other hand, for nuclei with large positive hexadecapole deformations, the optimum compact (or elongated) configuration (the orientation) has to be searched for the smallest (or largest) interaction radius R_B or, equivalently, the highest (or lowest) interaction barrier V_B for a hot (or cold) fusion reaction. In other words, the R_B at optimum orientations determines the compact hot and/or elongated cold configuration. Finally, in each case of the compact hot and elongated cold fusion processes, for choosing the best (compact or elongated) t-p combination, among the various predicted cold reaction valleys, the above-mentioned criterion of smallest interaction barrier, largest interaction radius, and nonnecked (no saddle) nuclear shapes must also then be satisfied. In this paper, we concentrate only on the case of compact hot fusion reactions.

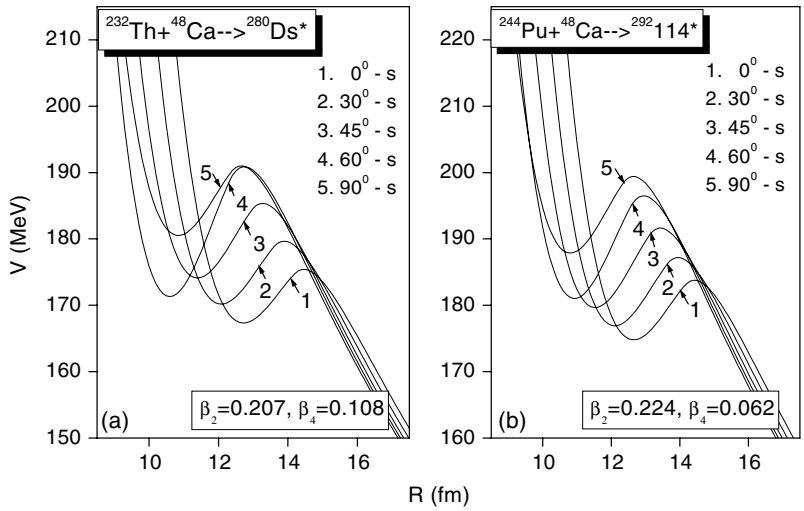

FIG. 2. Scattering potentials $V(R)$ for (a) ^{232}Th + ^{48}Ca $\rightarrow$ $^{280}_{110}$Ds* and (b) ^{244}Pu + ^{48}Ca $\rightarrow$ ^{292}114* reactions, at various orientations θ of the deformed target nuclei ^{232}Th and ^{244}Pu. Deformations are from Möller *et al.* [14].

III. CALCULATIONS AND RESULTS

We first calculated the scattering potentials *V(R)* for all the ^{48}Ca based reactions forming the excited compound systems Ds ($Z = 110$) to 118, including the still not experimentally studied ^{48}Ca + ^{224}Ra $\rightarrow$ $^{272}_{108}$Hs* reaction. This is illustrated in Fig. 2 for two cases of different deformations (one large β_4 and one small β_4), i.e., ^{232}Th + ^{48}Ca $\rightarrow$ $^{280}_{110}$Ds* and ^{244}Pu + ^{48}Ca $\rightarrow$ ^{292}114* reactions, respectively, calculated at some illustrative different orientations of the ^{232}Th and ^{244}Pu target nuclei. Concentrating only on the hot fusion process, we notice an interesting result: whereas in one case [Fig. 2(b)] the barrier at $\theta = 90^\circ$ is clearly the highest and its position most compact, in the other case [Fig. 2(a)], the $\theta < 90^\circ$ configuration competes with the one at $\theta = 90^\circ$. This result is better presented in Figs. 3 and 4, respectively, for the barrier positions R_B and barrier heights V_B as functions of the orientation angle θ of

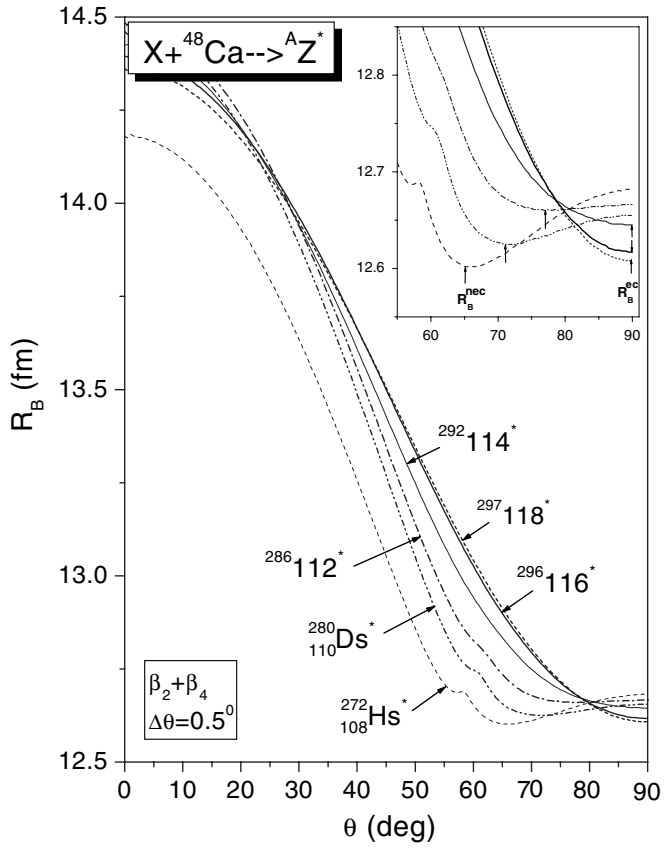

FIG. 3. Barrier positions R_B plotted as a function of the orientation angle θ of the deformed nucleus, for various ^{48}Ca based reactions forming compound systems with $Z = 108$–118. Deformations are included up to β_4, and angle θ is varied in a small step of 0.5°. In the inset, giving a magnified view of the narrow θ region around 90°, the minimum barrier positions R_B^{ec} and R_B^{nec} are also marked, pointing to the most compact configurations at $\theta = 90^\circ$ (ec) and $\theta < 90^\circ$ (nec), respectively.

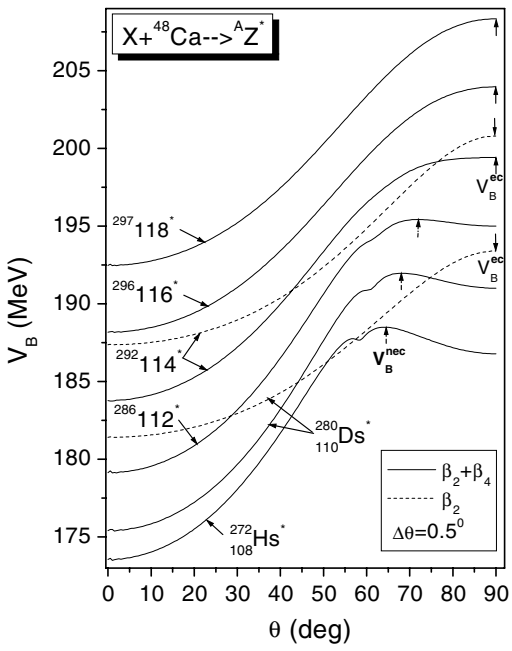

FIG. 4. Same as Fig. 3, but for barrier heights V_B. Positions of the optimum, i.e., highest barriers are also marked, pointing out the most compact configurations in Fig. 3. Thus, V_B^{ec} and V_B^{nec} refer, respectively, to compactness at $\theta = 90^\circ$ and $\theta < 90^\circ$. Also, cases of no hexadecapole deformation (dashed lines) are shown for comparisons.

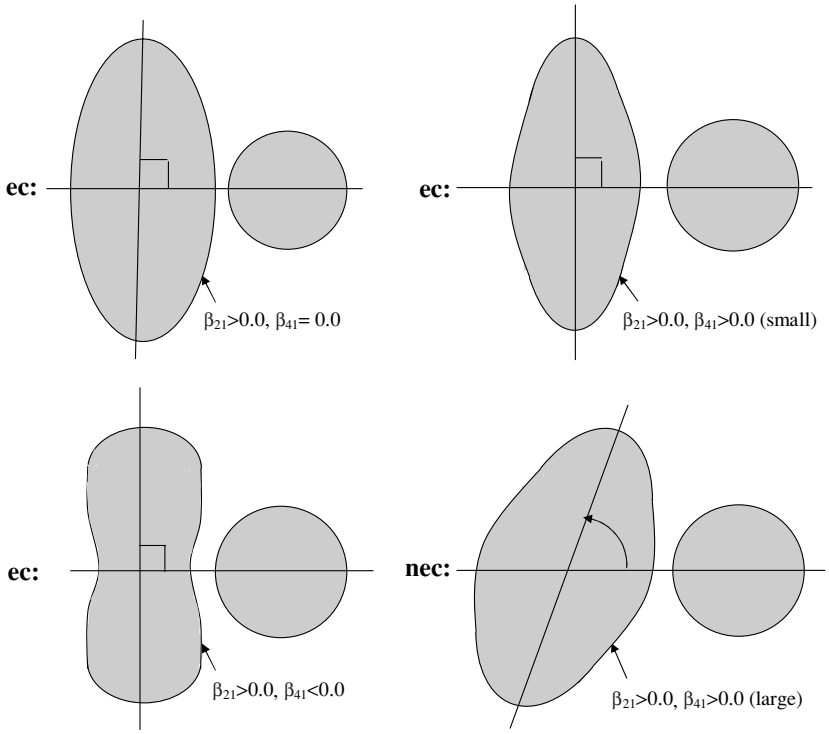

FIG. 5. Representative ec/nec hot fusion configurations of (prolate) deformed + spherical nuclei, for different magnitudes of hexadecapole deformations. The ec and nec refer, respectively, to the orientation of a deformed nucleus at $\theta = 90^\circ$ and $\theta < 90^\circ$.

the deformed reaction partner, for Hs ($Z = 108$) to 118 nuclei. Interestingly, for all $Z \geqslant 114$ nuclei, the barrier is highest and most compact (smallest R_B) at $\theta = 90^\circ$, the equatorial compact configuration, referred to as ($V_B^{\rm ec}$, $R_B^{\rm ec}$); and for all $Z < 114$, it is highest and most compact at $\theta < 90^\circ$, referred to as ($V_B^{\rm nec}$, $R_B^{\rm nec}$), the not-equatorial compact configuration. Note that the hot Hs compound nucleus also behaves very much like the other, already synthesized, heavier nuclei. This is further stressed in Table I (refer to experimental cases, the boldfaced ^{48}Ca based t-p combinations) where the deformations $\beta_{\lambda i}$ ($\lambda = 2, 3, 4$; $i = 1, 2$) and calculated barrier heights and positions are listed along with the compact configurations, the compact θ_i. Table I, and Figs. 3 and 4 show that for ^{48}Ca based reactions, the cases of equatorial compact (ec) and not-equatorial compact (nec) are clearly separated out. Fig. 5 illustrates some of these compact hot fusion configurations, which are further discussed below with respect to the different magnitudes of β_4. We notice in Fig. 5 (and Table I) that the nec configuration is considerably different from ec, the compact angle of orientation being $\sim 70^\circ$ for nec as compared to 90° for ec.

In Fig. 4, we also added our calculations for quadrupole deformation β_2 alone, for an illustrative case of each of the ec and nec reactions. Evidently, the hexadecapole deformation plays an important role, more so in the cases of nec fusion reactions: the ec $^{292}114^*$ remains ec, whereas the nec $^{280}_{110}$Ds* becomes ec for β_2 alone. Interestingly, with the addition of β_4 (here of positive sign), the barrier *decreases* at both $\theta = 0^\circ$ and 90°. Another important result that follows from Figs. 3 and 4 is the presence of a kink or cusp in all the nec, $Z < 114$ nuclei, representing some kind of a double humped barrier in the distribution of barriers with respect to the orientation angle θ, which becomes smooth as the compound nucleus Z increases, i.e., as one goes toward the higher-Z ($Z \geqslant 114$) ec reactions. Hence, clearly this property of barrier distribution in orientation angle must be related to the magnitudes of the quadrupole and hexadecapole deformations (see below).

Both the results of the separation between the ec and nec reactions and of the barrier distribution in the orientation angle are further presented in Figs. 6(a) and 6(b), respectively, in terms of the slopes

$$\Delta R_B/\Delta\theta \quad \text{and} \quad \Delta V_B/\Delta\theta \tag{14}$$

as a function of the final (higher) orientation angle θ, for the illustrative case of an ec (^{244}Pu + ^{48}Ca $\rightarrow$ $^{292}114^*$) and an nec (^{224}Ra + ^{48}Ca $\rightarrow$ ^{272}Hs*) reaction. This is done in order to amplify the effect of the presence of a cusp in Figs. 3 and 4 for $Z < 114$ nuclei. Note that the potential energy as a function of orientation angle is smooth (see Fig. 2 above or Fig. 4 in [11]), and so also is the barrier height and barrier position as a function of orientation angle in Figs. 3 and 4, except for a cusp at one fixed angle near the highest barrier or smallest interaction radius for $Z < 114$ nuclei. Note further that the angular step $\Delta\theta$ (=0.5°) in Figs. 3 and 4 is very small; hence, a small numerical instability in these calculations will be further magnified in the slopes $\Delta R_B/\Delta\theta$ and $\Delta V_B/\Delta\theta$. In order to reduce this effect, we plotted the slopes in Fig. 6 for a larger step of $\Delta\theta = 2^\circ$. In other words, though the small ripples in the curves of Fig. 6 are by no means of any physical significance, the minima-maxima effect is a representation of the cusp in Figs. 3 and 4 for $Z < 114$ nuclei. As $\Delta\theta$ decreases, both the ripples and the minima-maxima effect in the curves increase.

In Fig. 6, we notice that the slope changes sign if compactness changes from ec ($\theta = 90^\circ$) to nec ($\theta < 90^\circ$). Also, the barrier distribution in the orientation angle θ gets magnified

TABLE I. Target-projectile (t-p) combinations (A_1, A_2) referring to potential energy minima for compact hot compound systems (CS) and their characteristic properties. The ec, nec, bbc, near bbc, and nbbc stand, respectively, for equatorial (within $1-2^\circ$ deviation), not-equatorial, belly-to-belly, near belly-to-belly (within $5-6^\circ$ deviation), and not-belly-to-belly compact configurations. Boldfaced t-p combinations refer to experimental cases. ec and nec configurations refer to spherical + deformed t-p combinations. Angles θ_i are measured counter-clockwise.

CS	Reactions	Deformations of (A_1, A_2)						Barrier		Compact		Remark
	$(A_1 + A_2)$	β_{21}	β_{31}	β_{41}	β_{22}	β_{32}	β_{42}	V_B	R_B	θ_1	θ_2	
^{280}Ds	^{232}**Th** + ^{48}**Ca**	0.207	0.0	0.108	0.0	0.0	0.0	192.00	12.63	68°	s	nec
	^{226}Ra + ^{54}Ti	0.172	−0.1081[a]	0.112	0.0	0.0	0.0	202.70	12.86	90°	s	ec
	^{220}Rn + ^{60}Cr	0.111	−0.146	0.081	0.181	0.0	−0.021	216.43	12.83	90°	96°	near bbc
	^{208}Pb + ^{72}Ni	0.0	−0.013	0.0	0.053	0.0	0.009	237.04	13.15	s	91°	ec
	^{206}Hg + ^{74}Zn	−0.008	0.0	0.0	0.125	0.0	0.039	249.55	13.02	5°	90°	near bbc
	^{195}Os + ^{85}Se	0.127	0.0	−0.068	0.080	0.0	0.011	270.84	12.85	86°	91°	near bbc
	^{194}Os + ^{86}Se	0.145	0.0	−0.082	0.125	0.0	0.006	272.41	12.74	86°	91°	near bbc
	^{172}Dy + ^{108}Ru	0.286	0.0	−0.043	0.283	0.0	0.004	310.26	12.45	86°	90°	near bbc
	^{146}Ce + ^{134}Te	0.182	−0.1161[a]	0.080	0.0	0.0	0.0	308.09	13.23	90°	s	ec
^{286}112	^{238}**U** + ^{48}**Ca**	0.215	0.0	0.093	0.0	0.0	0.0	195.43	12.67	72°	s	nec
	^{236}U + ^{50}Ca	0.215	0.0	0.102	0.0	−0.015	0.0	194.74	12.72	71°	s	nec
	^{232}Th + ^{54}Ti	0.207	0.0	0.108	0.0	0.0	0.0	208.98	12.78	68°	s	nec
	^{226}Ra + ^{60}Cr	0.172	−0.108	0.112	0.181	0.0	−0.021	221.73	12.78	90°	96°	near bbc
	^{220}Rn + ^{66}Fe	0.111	−0.146	0.081	0.027	0.0	0.0	230.11	13.13	90°	90°	bbc
	^{208}Pb + ^{78}Zn	0.0	−0.013	0.0	0.089	0.0	0.003	253.57	13.15	s	90°	ec
	^{206}Hg + ^{80}Ge	−0.008	0.0	0.0	0.144	0.0	−0.033	264.57	13.10	4°	97°	near bbc
	^{194}Os + ^{92}Kr	0.145	0.0	−0.082	0.228	0.0	−0.019	288.02	12.73	86°	97°	near bbc
	^{180}Yb + ^{106}Mo	0.279	0.0	−0.098	0.361	0.0	−0.002	317.48	12.27	89°	95°	near bbc
	^{178}Yb + ^{108}Mo	0.279	0.0	−0.087	0.333	0.0	−0.027	316.71	12.31	89°	95°	near bbc
	^{152}Nd + ^{134}Te	0.262	0.0	0.128	0.0	0.0	0.0	319.83	13.17	74°	s	nec
^{292}114	^{244}**Pu** + ^{48}**Ca**	0.224	0.0	0.062	0.0	0.0	0.0	199.42	12.65	90°	s	ec
	^{242}Pu + ^{50}Ca	0.224	0.0	0.071	0.0	−0.015	0.0	198.47	12.71	89°	s	ec
	^{238}U + ^{54}Ti	0.215	0.0	0.093	0.0	0.0	0.0	212.77	12.81	72°	s	nec
	^{232}Th + ^{60}Cr	0.207	0.0	0.108	0.181	0.0	−0.021	228.17	12.71	71°	98°	nbbc
	^{222}Rn + ^{70}Ni	0.137	−0.132	0.100	0.027	0.0	0.0	246.74	13.18	90°	92°	near bbc
	^{220}Rn + ^{72}Ni	0.111	−0.146	0.081	0.053	0.0	0.009	246.27	13.21	90°	91°	near bbc
	^{210}Pb + ^{82}Ge	0.0	0.0	0.008[b]	0.053	0.0	0.001	267.53	13.32	52°	91°	nec
	^{206}Hg + ^{86}Se	−0.008	0.0	0.0	0.125	0.0	0.006	278.69	13.22	5°	91°	near bbc
	^{194}Os + ^{98}Sr	0.145	0.0	−0.082	0.357	0.0	0.056	305.43	12.63	86°	90°	near bbc
	^{192}W + ^{100}Zr	0.155	0.0	−0.082	0.358	0.0	0.039	313.18	12.62	85°	90°	near bbc
	^{184}Hf + ^{108}Mo	0.260	0.0	−0.128	0.333	0.0	−0.027	326.09	12.30	90°	94°	near bbc
	^{158}Sm + ^{134}Te	0.279	0.0	0.082	0.0	0.0	0.0	330.05	13.16	0°	s	ec
^{296}116	^{248}**Cm** + ^{48}**Ca**	0.235	0.0	0.040	0.0	0.0	0.0	203.97	12.62	90°	s	ec
	^{246}Cm + ^{50}Ca	0.234	0.0	0.057	0.0	−0.015	0.0	202.78	12.70	90°	s	ec
	^{242}Pu + ^{54}Ti	0.224	0.0	0.071	0.0	0.0	0.0	217.24	12.78	89°	s	ec
	^{236}U + ^{60}Cr	0.215	0.0	0.102	0.181	0.0	−0.021	232.73	12.73	72°	98°	nbbc
	^{220}Rn + ^{76}Zn	0.111	−0.146	0.081	0.142	0.0	0.033	264.36	13.16	90°	90°	bbc
	^{210}Pb + ^{86}Se	0.0	0.0	0.008[b]	0.125	0.0	0.006	284.63	13.28	52°	91°	nec
	^{208}Pb + ^{88}Se	0.0	−0.013	0.0	0.181	0.0	−0.012	286.00	13.19	s	92°	ec
	^{206}Pb + ^{90}Se	−0.008	0.0	−0.008	0.220	0.0	−0.045	286.96	13.13	0°	96°	near bbc
	^{194}Os + ^{102}Zr	0.145	0.0	−0.082	0.369	0.0	0.017	319.60	12.71	84°	90°	near bbc
	^{190}W + ^{106}Mo	0.173	0.0	−0.097	0.361	0.0	−0.002	328.49	12.62	86°	95°	near bbc
	^{162}Gd + ^{134}Te	0.291	0.0	0.043	0.0	0.0	0.0	340.96	13.14	90°	s	ec

[a]This case of large β_{41} behaves like a case of small β_{41} (giving ec configuration) because of nonzero β_{31}.

[b]^{210}Pb is a spherical nucleus ($\beta_{21} = 0.0$) and hence should be a case of ec, but it is obtained as nec because it has $\beta_{41} > 0$ [14]. The presence of even small β_{41} in a spherical nucleus seems to have a large effect on compact orientation.

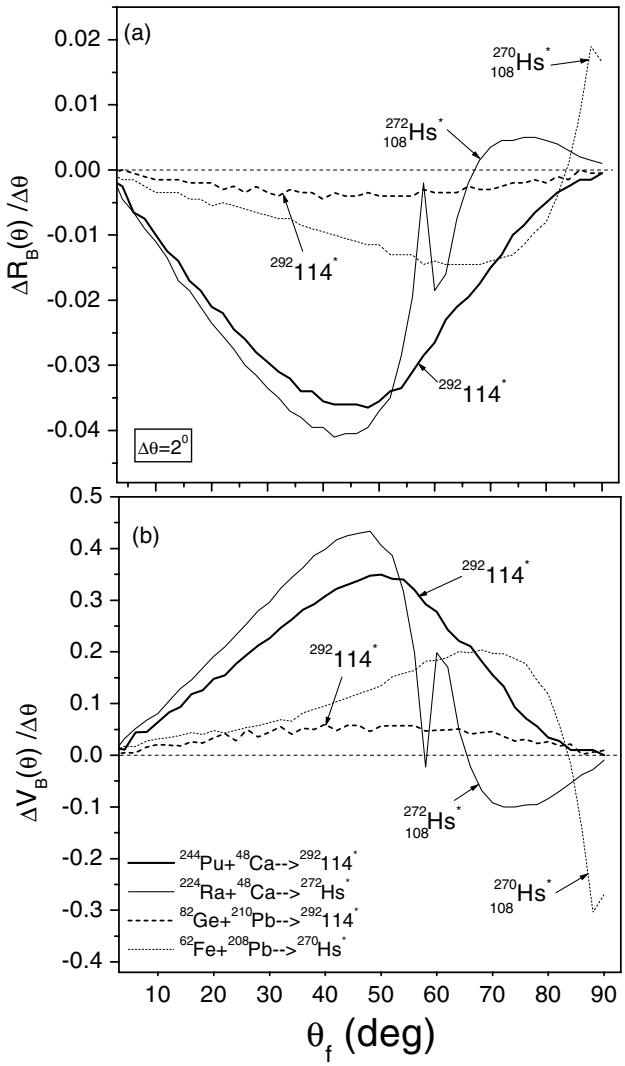

FIG. 6. Slopes (a) $\Delta R_B/\Delta\theta$ and (b) $\Delta V_B/\Delta\theta$ as functions of the final (higher) orientation angle θ for two ^{48}Ca based reactions, illustrating ec and nec configurations. Also, cases of ^{208,210}Pb based reactions are plotted for comparison.

from one of a smooth to that of a strong minima (maxima) effect. We have also shown in Fig. 6 the calculations for two (spherical) Pb based reactions ^{82}Ge + ^{210}Pb → ^{292}114* and ^{62}Fe + ^{208}Pb → $^{270}_{108}$Hs*, which clearly present, respectively, the case of the ec and nec configuration for hot fusion reactions. Apparently, we obtain the same result for Pb based reactions as for the ^{48}Ca based reactions. In other words, the division between ec and nec hot fusion and, hence, the barrier distribution effect seem to be independent of the choice of spherical (^{48}Ca or ^{208,210}Pb)-plus-deformed reaction partners (t-p combinations).

The next question is: What is the cause for such a division between the ec and nec configurations. In the following, we show that this occurs because of the combined effects of the magnitudes of their quadrupole and hexadecapole deformations, with the magnitude of the hexadecapole deformation playing the major role.

Figure 7 gives a plot of barrier position R_B^{ec} at equatorial compact configuration ($\theta = 90^\circ$) with respect to its position R_B^c at any (ec or nec) compact configuration, i.e., the difference $R_B^{ec} - R_B^c$ as a function of the quadrupole deformation β_2 and hexadecapole deformation β_4 of the deformed reaction partner, for all the Hs ($Z = 108$) to 118 nuclei considered above. Note that for $Z \geqslant 114$, the R_B^{ec} itself is the compact, configuration; hence, the difference $R_B^{ec} - R_B^c$ is zero, whereas for $Z < 114$, $R_B^c < R_B^{ec}$. Similarly, Fig. 8 gives the same plot for barrier height V_B^{ec}, i.e., the difference $V_B^{ec} - V_B^c$ as a function of β_2 and β_4 of the deformed nucleus. It is interesting to observe that the nuclei with larger quadrupole deformation and smaller hexadecapole deformation are a separate class, having an equatorially compact configuration, and that this compactness shifts to $\theta < 90^\circ$ as β_2 decreases or β_4 increases.

The above observation has an interesting consequence if we increase or decrease the magnitudes of β_2 and β_4, more so for β_4 (including the negative β_4 values), beyond what is involved above in Figs. 7 and 8. This is illustrated in Fig. 9, for R_B calculated for different orientation angle θ values and varying β_4 arbitrarily from -0.15 to $+0.15$ values, in the reactions ^{224}Ra + ^{48}Ca → $^{272}_{108}$Hs* and ^{244}Pu + ^{48}Ca → ^{292}114*, representing the case each of the nec and ec

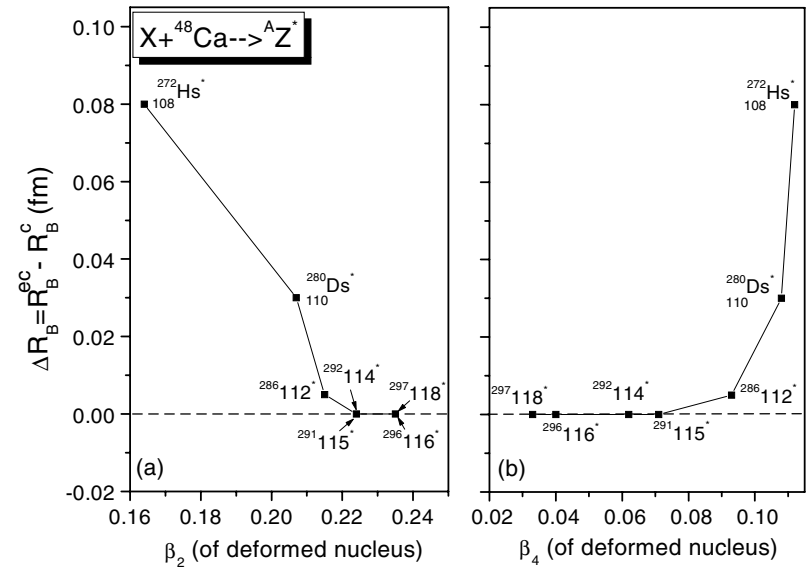

FIG. 7. Difference $R_B^{ec} - R_B^c$, between barrier position R_B^{ec} at equatorial configuration ($\theta = 90^\circ$) and its position R_B^c at any compact (ec or nec) configuration, as a function of (a) the quadrupole deformation β_2 and (b) hexadecapole deformation β_4 of deformed reaction partner, for $Z = 108$–118 nuclei.

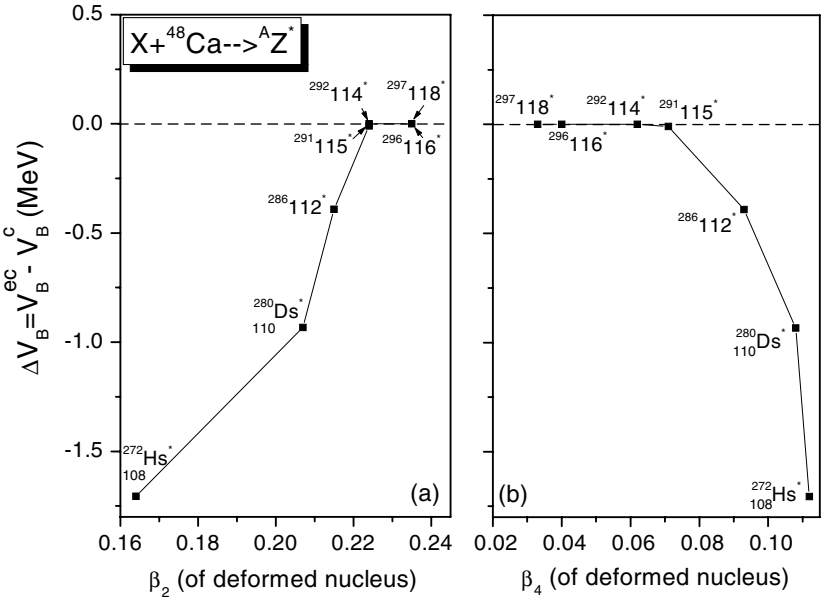

FIG. 8. Same as Fig. 7, but for barrier height V_B.

configurations. Similarly, Fig. 10 shows the same calculation for β_2 varied in the neighborhood of the values of the deformed partners in the above reactions. Evidently, the results in both Figs. 9 and 10 are very sensitive to the choice of deformation parameters β_2 and β_4. In Fig. 9, for both the cases of small and large quadrupole deformations, except for an inflection point at the negative β_4 value in the case of smaller β_2, the ec ($\theta = 90^\circ$) configurations are obtained only for small β_4 values, becoming better and better for negative β_4 values. The inflection point manifests the role of the nec configuration occurring in the neighborhood of $\theta = 90^\circ$ (in this case 88°) at a particular (negative) β_4 value for target nucleus with smaller β_2 value, as illustrated in the inset of Fig. 9(a). This is further discussed below and occurs in all $Z < 114$ nuclei. On the other hand, Fig. 10 shows that for the case of large positive β_4, the ec configurations become possible only for the larger β_2 values, and that for the smaller positive β_4 case, the ec configurations occur even at smaller β_2 values.

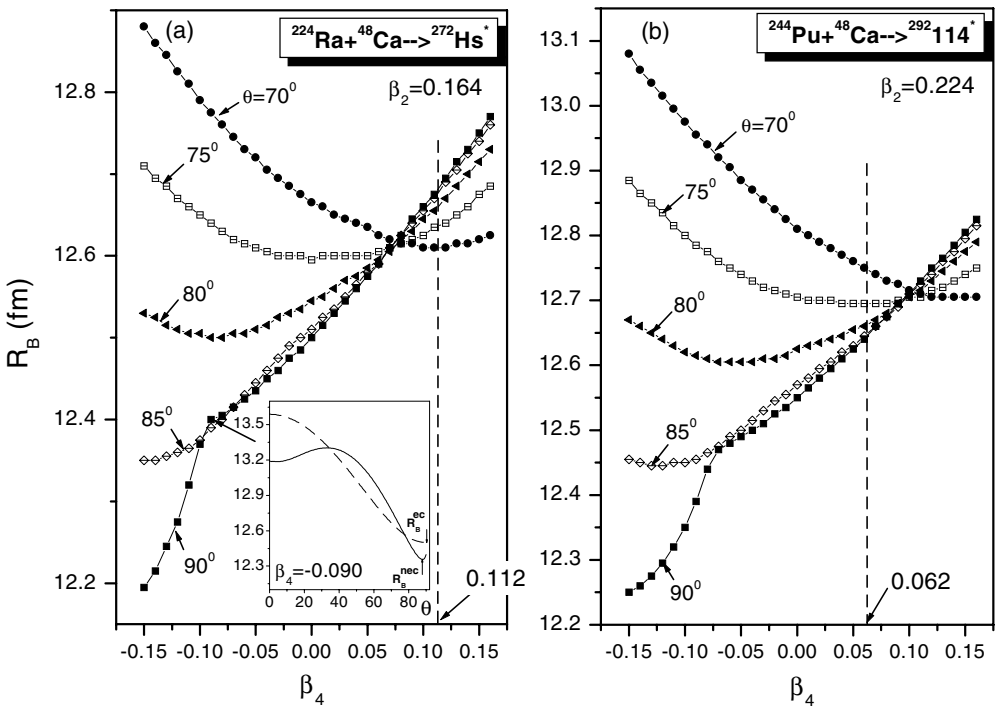

FIG. 9. Barrier position R_B as a function of the hexadecapole deformation parameter β_4, for different orientation angles θ, calculated for the reactions (a) ^{224}Ra + ^{48}Ca → ^{272}Hs* and (b) ^{244}Pu + ^{48}Ca → ^{292}114*. β_2 values of ^{224}Ra and ^{244}Pu are also marked. Inset shows the variation of barrier position w.r.t. orientation angle at the inflection point for both the case of β_2 alone and with β_4 added.

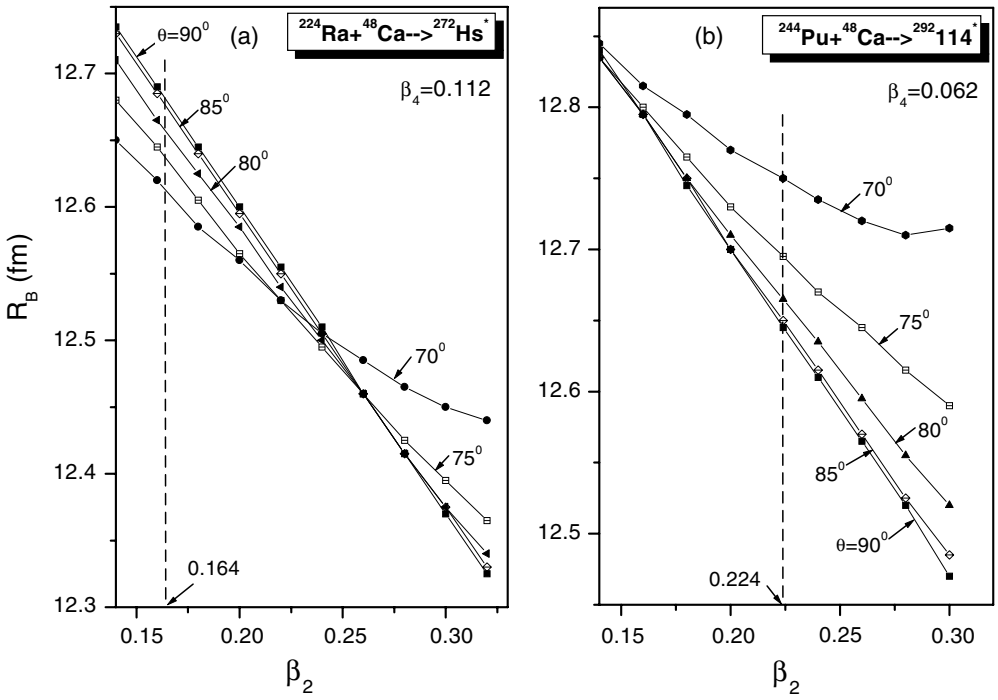

FIG. 10. Same as Fig. 9, but as a function of the quadrupole deformation parameter β_2.

As already noted above in Fig. 9, the case of *large* negative β_4 is of specific interest for ec configurations, which is best exemplified in Fig. 11 for the reaction $^{184}\mathrm{W} + {}^{48}\mathrm{Ca} \rightarrow {}^{232}_{94}\mathrm{Pu}^*$,

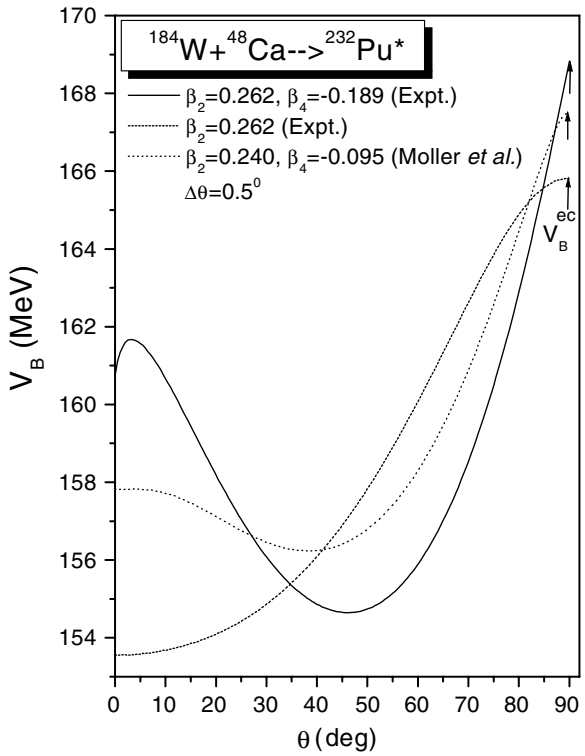

FIG. 11. Same as Fig. 4, but for the reaction $^{184}\mathrm{W} + {}^{48}\mathrm{Ca} \rightarrow {}^{232}_{94}\mathrm{Pu}^*$, using the data for deformations from experiments [23] and from Möller *et al*. [14].

where ^{184}W has the measured [23] large prolate deformation and large negative hexadecapole deformation. Apparently, in Fig. 11, the highest barrier is for the ec configuration, which is not affected (except for its height) by the inclusion of this small hexadecapole deformation. The same result holds good for the case of a smaller prolate deformation with large negative hexadecapole deformation, as is evident in Fig. 9. Of course, as already observed in [1], the addition of the hexadecapole deformation is important for studying the barrier characteristics, such as the barrier distribution with respect to the orientation angle. Note that the characteristics of barrier distribution in orientation degrees of freedom due to the addition of β_4 with a negative sign in Fig. 11 are reverse to those of Fig. 4 (or Fig. 3) where β_4 is of positive sign. Here in Fig. 11, the barrier is increased at both the 0° and 90° orientations, whereas the same in Fig. 4 are decreased because of the addition of β_4. This shift in barrier height (equivalently, in position) due to the addition of positive or negative β_4 leads to the above-noted inflection point, related to the barrier distribution in the neighborhood of 90°, more so for nec configurations.

Next, for a given compound nucleus, we calculated the fragmentation potential for the optimum orientations of different t-p combinations forming compact hot fusion configurations. This is given in Figs. 12 and 13, calculated at $R = R_B$ and optimum orientations for each t-p combination (η value) forming the compact hot compound systems $^{280}_{110}$Ds*, ^{286} 112*, ^{292} 114*, and ^{296}116*. Thus, $R = R_B$ at optimum orientations defines the compact configuration, calculated for each t-p combination. Such a calculation needed large computer time, since this meant searching for a configuration with the shortest distance s_0 for each pair of the oriented colliding nuclei, consisting of both spherical + (prolate/oblate) deformed and

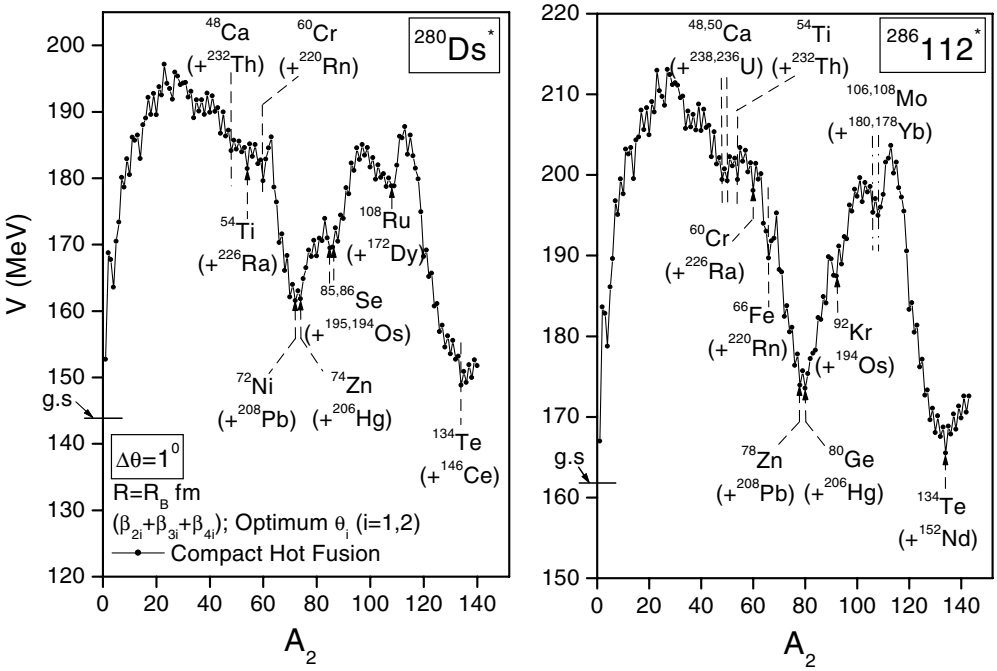

FIG. 12. Fragmentation potentials for the optimally oriented compact hot fusion of different t-p combinations, with $\lambda = 2, 3, 4$, forming $^{280}_{110}$Ds* and $^{286}112^*$. g.s. denotes the ground state energy.

deformed+deformed t-p combinations. We made this search in steps of $\Delta\theta = 1^\circ$.

We notice in Figs. 12 and 13 that in addition to a minimum at ^{48}Ca (also at its neighbor ^{50}Ca in some cases, which is radioactive), a number of other reaction valleys (minima) occur, including the one at an isotope of Pb. The resulting t-p combinations are listed in Table I, along with their other characteristics, such as the deformations, R_B, V_B, and compact orientations θ_i. We find that R_B values are, on the average, larger than the touching radii $R_T = R_{01} + R_{02}$ by $\sim$1.5 fm.

Table I shows that the equatorial (within $\sim$1–2° of deviation, for deformed + spherical t-p combinations) and belly-to-belly (or near belly-to-belly within $\sim$5$-$6° of

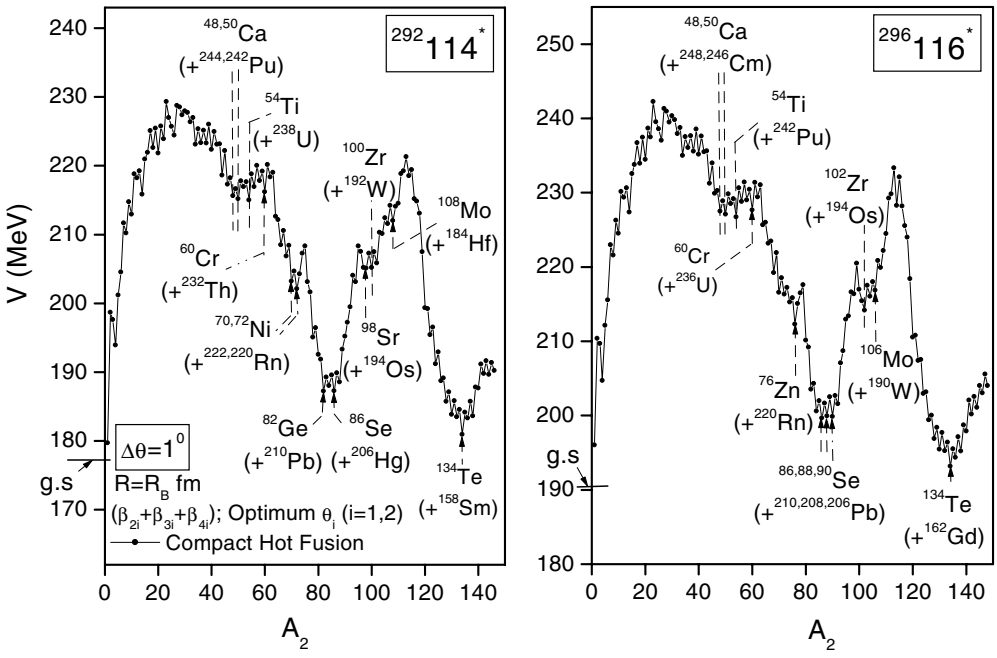

FIG. 13. Same as Fig. 12, but for $^{292}114^*$ and $^{296}116^*$.

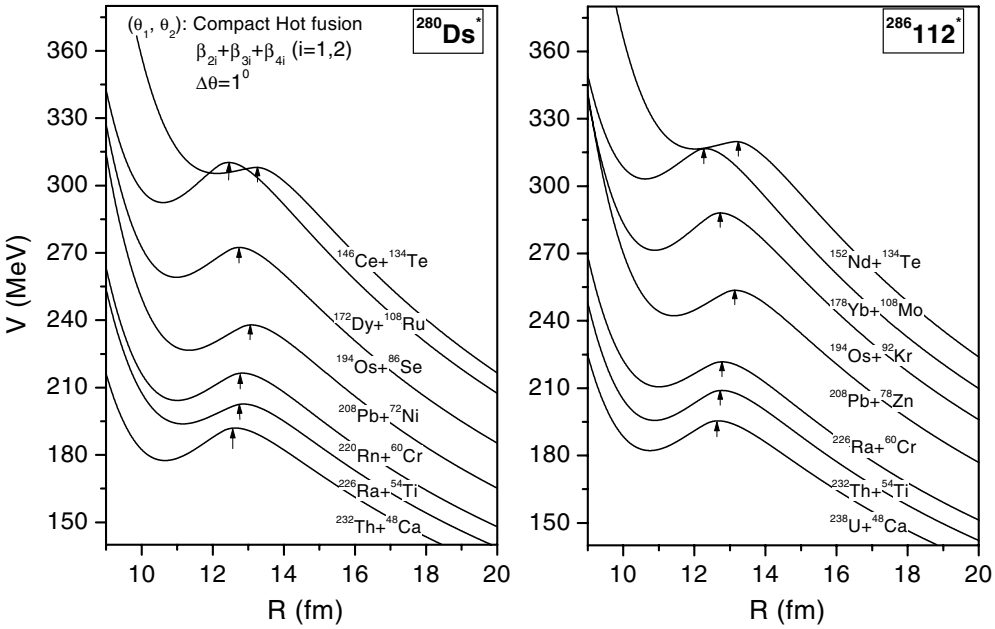

FIG. 14. Same as Fig. 2, but for different t-p combinations listed in Table I, referring to minima in the optimally oriented compact hot fusion potential energy surface of Fig. 12. Arrows indicate barrier positions.

deviation, for deformed + deformed t-p combinations) are the most compact configurations (denoted, ec and bbc). Then, some configurations are neither equatorial (nec) nor belly-to-belly compact (nbbc), which happens because one of the hexadecapole deformations (β_{41} or β_{42}) is large positive. We find that the analysis carried out in the earlier part of this paper for spherical + deformed nuclei is nearly applicable to deformed + deformed nuclei. We also notice in Table I that in some cases, the nonzero β_3 also plays an important role, as in the ^{226}Ra + ^{54}Ti $\rightarrow$ $^{280}_{110}$Ds* reaction, the ^{226}Ra has large $+\beta_4$ but because of $\beta_3 \neq 0$, it behaves as one with small β_4 (the role of β_3 is still to be investigated in detail). The corresponding compact shapes for both ec and nec cases are shown in Fig. 5. This serves to identify the cases of β_2 alone (zero β_4), small positive β_4 or large negative β_4, and the large positive β_4, independent of (small or large) β_2 values, respectively, for ec and nec configurations. Similar configurations, as those in Fig. 5 for spherical + deformed nuclei, are evident from

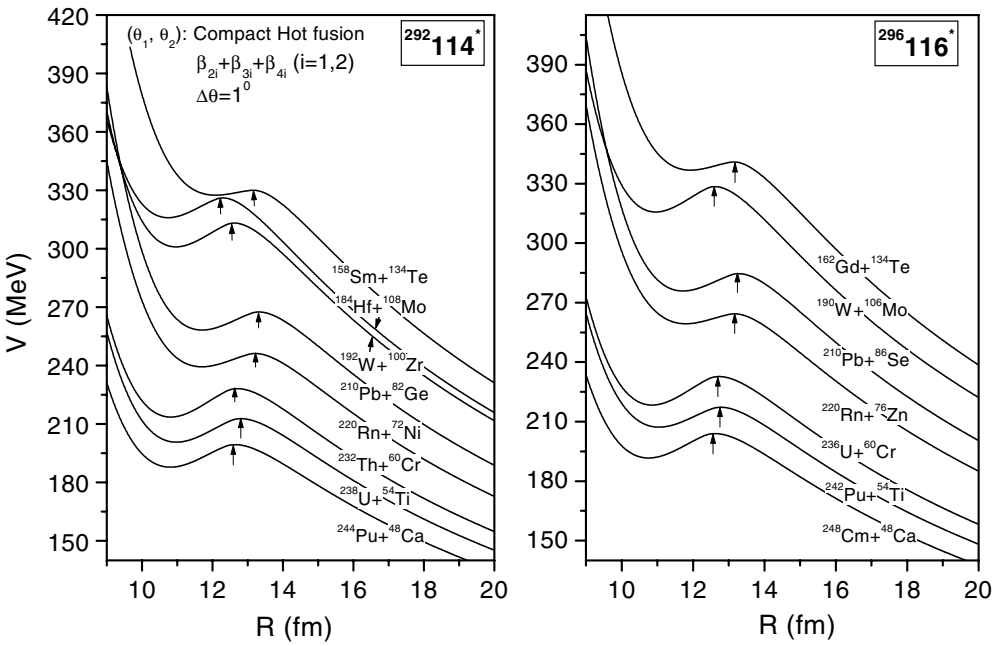

FIG. 15. Same as Fig. 14, but referring to potential energy surface of Fig. 13.

Table I for deformed + deformed nuclei which are known to form belly-to-belly configurations for hot fusion reactions [1]. The differences in the compact orientation angles between the bbc and nbbc are again found to be significantly large ($\sim 20^\circ$), though most of the configurations are near bbc. Also, as for β_3 mentioned above, the role of multipole deformations higher than β_4 could be significant and need further investigation.

Finally, Figs. 14 and 15 give the scattering potentials for a few representative t-p combinations listed in Table I, referring to the optimally oriented compact hot fusion of $Z = 110$–116 compound systems. It is apparent from these figures that the barrier is always lowest for ^{48}Ca induced cases, though the barrier position is a bit more elongated for the next best cold reaction valley based on a ^{54}Ti beam. This means that relatively speaking the Ca induced reactions are the best cold fusion reactions with optimum orientations of ec or nec hot fusion, depending on the mass and charge of the compound system and the magnitude of hexadecapole (β_4) deformation of the deformed reaction partner. Also, in each case, another cold fusion reaction of equal interest is the neighboring reaction induced on the actinides (^{226}Ra, ^{232}Th, ^{238}U, and ^{242}Pu) by ^{54}Ti, the next heavier beam to the ^{48}Ca beam. Such actinide based reactions are planned to be carried out soon at GSI (Darmstadt).

IV. SUMMARY AND DISCUSSION

In this paper, we used the extended fragmentation theory for deformed and oriented nuclei to understand further the phenomenon of compactness, i.e., the collisions at 90° orientation or, equivalently, in the direction of the minor axis of the deformed nucleus, observed in ^{48}Ca induced hot fusion reactions on actinides, with a view to analyze for the first time the role of the magnitudes of quadrupole and hexadecapole deformations on the orientation degrees of freedom. This study includes the experimentally synthesized hot fusion compound systems ^{110}Ds to $Z = 118$ and the not-yet experimentally studied hot fusion reactions with the ^{48}Ca beam on, e.g., W and Ra, and the already used Pb based reactions of cold fusion studies.

Knowing that all hot fusion reactions are compact [1,4] (highest barrier and smallest interaction radius), we have found that all compound systems with $Z \geqslant 114$ are compact at the orientation angle $\theta = 90^\circ$ (collisions in the direction of the minor axis of the deformed nucleus), the so-called equatorial compact (ec) configuration, and that the same for $Z < 114$ are compact at $\theta < 90^\circ$, referred to as the not-equatorial compact (nec) configuration. This result of the barrier distribution in orientation degrees of freedom is similar to what was observed by Misicu and Greiner [7], based on the calculations of the capture cross sections and fusion-barrier distribution [24]. The ec configuration refers to the total contribution of the barrier at one angle ($\theta = 90^\circ$) and the same for nec occurs for barriers at two (or more) angles. This result is understood in terms of the magnitudes of both the quadrupole and hexadecapole deformations: Whereas the pure quadrupole deformed nuclei and the nuclei with normal (large or small) quadrupole deformation plus small-positive or negative hexadecapole deformation result in an ec configuration, the ones with normal (large or small) quadrupole deformation plus large-positive hexadecapole deformation gives rise to an nec configuration. This result for spherical + deformed nuclei is summarized in Fig. 5, stressing the role of the relative magnitudes of hexadecapole deformation for the first time. The same result is true for deformed + deformed nuclei. Of course, the other multipole deformations (not considered here) may also be important, but not much experimental or theoretical information is available for the octupole deformations and deformations higher than the hexadecapole deformation.

Finally, the calculated fragmentation potential, using optimum orientations of compact hot fusion reactions, gives rise to various cold reaction valleys, which always include ^{48}Ca, ^{54}Ti, ^{60}Cr, ^{208,210}Pb, and many other spherical + deformed and deformed + deformed reaction partners. These minima include both ec and nec configurations, as well as the bbc (near bbc) and nbbc configurations. This information on cold target-projectile combinations, optimized in terms of the calculated scattering potentials show that ^{48}Ca and ^{54}Ti induced reactions on various actinides are the two best cold fusion reactions with optimum orientations of the hot fusion process.

ACKNOWLEDGMENTS

This work is supported in part by Deutsche Forschungsgemeinschaft (DFG), Germany, and Council of Scientific and Industrial Research (CSIR), New Delhi, India, which is gratefully acknowledged.

[1] R. K. Gupta, M. Balasubramaniam, R. Kumar, N. Singh, M. Manhas, and W. Greiner, J. Phys. G: Nucl. Part. Phys. **31**, 631 (2005), and references therein.

[2] R. K. Gupta, N. Singh, and M. Manhas, Phys. Rev. C **70**, 034608 (2004).

[3] M. Manhas and R. K. Gupta, Phys. Rev. C **72**, 024606 (2005).

[4] R. K. Gupta, M. Manhas, G. Münzenberg, and W. Greiner, Phys. Rev. C **72**, 014607 (2005).

[5] Yu. Ts. Oganessian, V. K. Utyonkov, Yu. V. Lobanov, F. Sh. Abdullin, A. N. Polyakov, I. V. Shirokovsky, Yu. S. Tsyganov, G. G. Gulbekian, S. L. Bogomolov, B. N. Gikal, A. N. Mezentsev, S. Iliev, V. G. Subbotin, A. M. Sukhov, A. A. Voinov, G. V. Buklanov, K. Subotic, V. I. Zagrebaev, M. G. Itkis, J. B. Patin, K. J. Moody, J. F. Wild, M. A. Stoyer, N. J. Stoyer, D. A. Shaughnessy, J. M. Kenneally, and R. W. Lougheed, Phys. Rev. C **69**, 054607 (2004).

[6] Yu. Ts. Oganessian, V. K. Utyonkov, Yu. V. Lobanov, F. Sh. Abdullin, A. N. Polyakov, I. V. Shirokovsky, Yu. S. Tsyganov, G. G. Gulbekian, S. L. Bogomolov, B. N. Gikal, A. N. Mezentsev, S. Iliev, V. G. Subbotin, A. M. Sukhov, A. A. Voinov, G. V. Buklanov, K. Subotic, V. I. Zagrebaev, M. G. Itkis, J. B. Patin, K. J. Moody, J. F. Wild, M. A. Stoyer, N. J. Stoyer,

D. A. Shaughnessy, J. M. Kenneally, P. A. Wilk, R. W. Lougheed, R. I. Il'kaev, and S. P. Vesnovskii, Phys. Rev. C **70**, 064609 (2004).
[7] S. Misicu and W. Greiner, Phys. Rev. C **69**, 054601 (2004).
[8] S. Misicu and W. Greiner, Phys. Rev. C **66**, 044606 (2002).
[9] A. Iwamoto, P. Möller, J. R. Nix, and H. Sagawa, Nucl. Phys. **A596**, 329 (1996).
[10] W. Nörenberg, GSI Nachrichten 10-94 (1994), p. 13; in *Proceedings of International Workshop on Heavy Ion Fusion*, Padava, Italy (World Scientific, Singapore, 1994), p. 248.
[11] V. Yu. Denisov and W. Nörenberg, Eur. Phys. J. A **15**, 375 (2002).
[12] M. J. Rhoades-Brown and V. E. Oberacker, Phys. Rev. Lett. **50**, 1435 (1983).
[13] J. Fernández-Niello and C. H. Dasso, Phys. Rev. C **39**, 2069 (1989).
[14] P. Möller, J. R. Nix, W. D. Myers, and W. J. Swiatecki, At. Data Nucl. Data Tables **59**, 185 (1995).
[15] G. Audi and A. H. Wapstra, Nucl. Phys. **A595**, 4 (1995).
[16] H. J. Fink, W. Greiner, R. K. Gupta, S. Liran, H. J. Maruhn, W. Scheid, and O. Zohni, in *Proceedings of the International Conference on Reactions between Complex Nuclei*, Nashville, 1974, edited by F. K. McGowan, J. B. Ball, and J. H. Hamilton (North-Holland, Amsterdam, 1974), Vol. 2, p. 21.
[17] J. Maruhn and W. Greiner, Phys. Rev. Lett. **32**, 548 (1974).
[18] R. K. Gupta, W. Scheid, and W. Greiner, Phys. Rev. Lett. **35**, 353 (1975).
[19] A. Sandulescu, R. K. Gupta, W. Scheid, and W. Greiner, Phys. Lett. **B60**, 225 (1976).
[20] R. K. Gupta, Sovt. J. Part. Nucl. **8**, 289 (1977).
[21] R. K. Gupta, in *Heavy Elements and Related New Phenomena*, edited by W. Greiner and R. K. Gupta (World Scientific, Singapore, 1999), Vols. I and II, Chap. 10 and 14.
[22] R. K. Gupta, A. Sándulescu, and W. Greiner, Phys. Lett. **B67**, 257 (1977).
[23] I. Y. Lee, J. X. Saladin, J. Holden, J. O'Brien, C. Baktash, C. Bemis, Jr., P. H. Stelson, F. K. McGowan, W. T. Milner, J. L. C. Ford, Jr., R. L. Robinson, and W. Tuttle, Phys. Rev. C **12**, 1483 (1975).
[24] N. Rowley, G. R. Satchler, and P. H. Stelson, Phys. Lett. **B254**, 25 (1991).